Particle acceleration in cascading current sheet

D. Kramoliš[1], M. Bárta[2], M. Varady[1,2]

[1] Department of Physics, J.E. Purkyně University, České mládeže 8, 400 24 Ústí nad Labem, Czech Republic
[2]Astronomický ústav Akademie věd České republiky, v.v.i, Fričova 298, 251 65 Ondřejov, Czech Republic

Abstract

The aim of our research is to study the mechanisms and efficiency of electron acceleration in the coronal current sheets using test-particle approach. In our work, we compute particle trajectories using the relativistic Guiding Centre Approximation (GCA) method combined with the relativistic full-orbit (F-O) algorithm, to treat the regions where GCA fails, in the precomputed time-dependent electromagnetic fields obtained from MHD simulations. At the present stage, an acceleration in the reconnecting current sheet with fractal topology (Bárta et. al. 2011) is investigated using two various scales of resistivity. We present preliminary results where we identify the main regions of particle acceleration in the coronal current sheet with fractal topology.

Model desription

- Current sheet time evolution: 2.5D MHD simulation of cascading reconnection (Bárta et al. 2011) scaled towards dissipative scale of magnetic reconnection ($\sim$ 10 m) (Fig. 1, 2, 3), space dimensions $\sim (6 \times 10^4, 7 \times 10^3, 6 \times 10^4)$ m, evolution time $\sim 3 \times 10^{-4}$ s.
- An important aspect of our model is that it covers only the smallest spatial scales of the fractal cascade of plasmoids. Large scale current sheets in flares comprise a large number of such structures.
- MHD simulations performed in dimensionless units - results converted to SI units (Bárta, private communication).
- **E**, **B** interpolated to current particle position and time using linear interpolation. Convective electric field $\mathbf{E}_{\rm conv}$ is kept perpendicular to **B** during interpolation.
- Conductive electric field $\mathbf{E}_{\rm res}$ (Fig. 1) depends on anomalous resistivity (Büchner et al. 2006), according to kinetic simulations of solar flares $K_{\rm res} \approx 10 - 1000$,

$$T_0 = 2 \times 10^6 \text{ K}\,,\ B_0 = 0.04 \text{ T}\,,\ L_{\rm A} = 6.0 \times 10^5 \zeta \text{ m}\,,$$
$$\eta_0 = 0.01 K_{\rm res} \frac{jc}{nc_{\rm S}} \frac{1}{\epsilon_0 \lambda_{ie} \omega_{\rm pi}^2 L_{\rm A}} \frac{1}{\eta_{\rm max}}\,,$$
$$\mathbf{E}_{\rm res} = \frac{\eta_0 B_0}{\mu_0 L_{\rm A}} \mathbf{j}\,,$$

where T_0, B_0, $L_{\rm A}$ are initial temperature, field, current-sheet width in MHD model, $\omega_{\rm pi}$ is ion plasma frequency, η_0 is scaling factor for resistivity computed in region with $\eta_{\rm max}$, λ_{ie} is proton to electron mass ratio, n, j are local dimensionless density and current and $\zeta = 1/3000$ is down-scaling factor to dissipative scale.

- Algorithms: Switching between relativistic GCA (e.g. Northrop 1963, Gordovskyy et al. 2010) and full-orbit pusher (Hyman 1997, Vay 2008), periodic BC.
- Test particles: Electrons with initial energy given by a shifted Maxwell distribution corresponding to local electron temperature + bulk drift velocity (Fig. 3), generated randomly along the current sheet in a vertical band (width 400 m i.e. 5% of the simulation box width – see red dashed lines in Figure 2). Number of generated particles is weighted using the local density profile (see Figure 2).
- Timesteps:
  - For GCA:

$$\Delta t_{\rm GCA} = \frac{1}{5} \frac{L_{\rm c}}{v}\,,$$

    where L_c is size of MHD data cell.
  - For F-O (fraction of gyroperiod):

$$\Delta t_{\rm F-O} = \frac{1}{20} \frac{2\pi\gamma m}{|q|B}\,.$$

    The total time spent on full-orbit during a single run is

$$t_{\rm F-O} = \min(\Delta t_{\rm GCA}, 1000 \Delta t_{\rm F-O}(0))\,,$$

    so particle goes through approximately 50 orbits.
- Switching conditions:
  - GCA step is performed when all following conditions are fulfilled

$$\Delta\alpha < \frac{\pi}{4}\,,$$
$$|\nabla B|_\perp < \tfrac{1}{10}\tfrac{B}{r_{\rm L}} \quad \Rightarrow \quad |\nabla B|_\perp < \tfrac{1}{10}\left|\tfrac{qB^2}{\gamma m v_\perp}\right|\,,$$
$$|\nabla B|_{||} < \tfrac{1}{10}\tfrac{\omega_{\rm L} B}{v_{||}} \quad\quad\ \ |\nabla B|_{||} < \tfrac{1}{10}\left|\tfrac{qB^2}{\gamma m v_{||}}\right|\,,$$

    where $\Delta\alpha$ is difference between old and new pitch angle of particle, $r_{\rm L}$ Larmor radius and $\omega_{\rm L}$ gyrofrequency. Otherwise F-O algorithm is used.
  - Before the full-orbit pusher is used, particle is moved from it's guiding centre (GC) to it's real position (using randomly rotated vector around **B**). At the end of F-O run, the velocity of particle is averaged over the last orbit (to treat the influence caused by $\mathbf{E} \times \mathbf{B}$ drift) and the particle is moved back to GC.

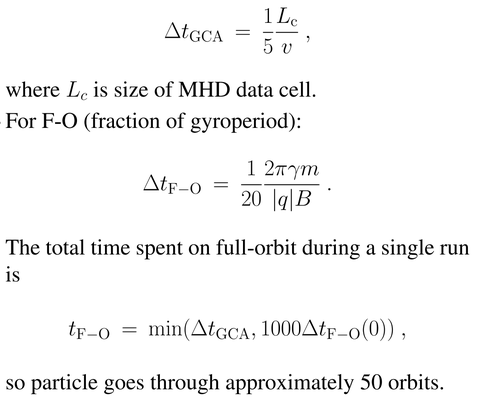

Figure 1: Conductive electric field at the start of simulation for $K_{\rm res} = 100$.

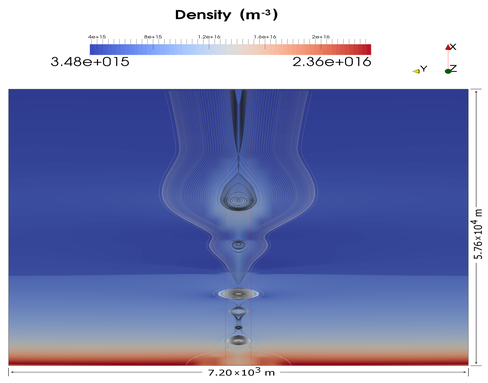

Figure 2: Density profile at the start of simulation. Vertical red dashed lines show the region of test particle generation.

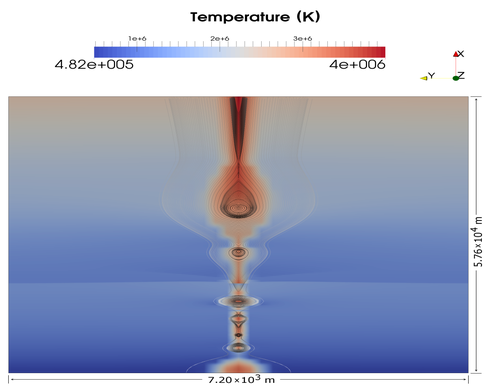

Figure 3: Temperature profile at the start of simulation.

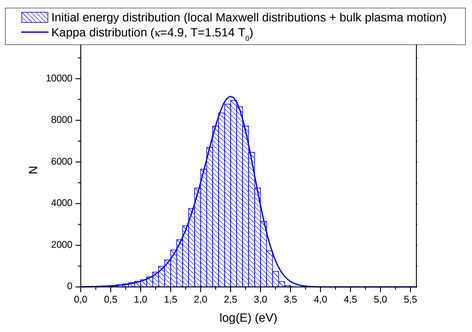

Figure 4: Initial electron energy distribution.

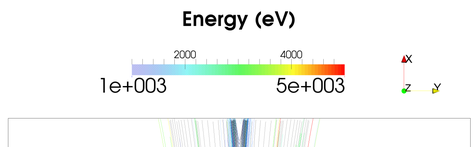

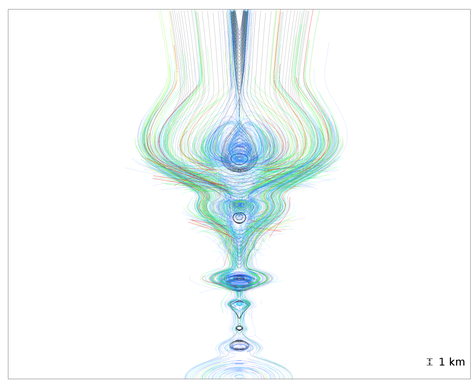

Figure 11: Particle trajectories with colour coded particle energy for $K_{\rm res} = 10$ (Turbulent mode). Grey lines show the initial magnetic field.

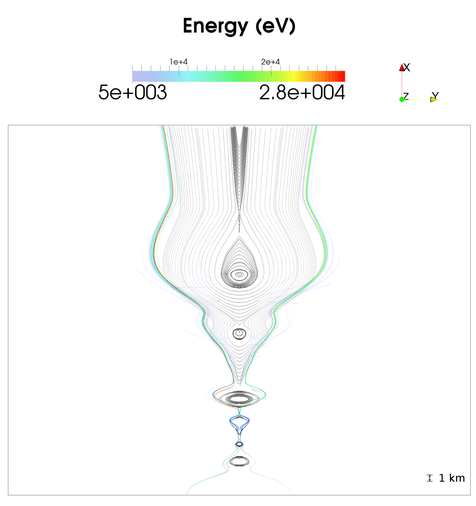

Figure 12: Particle trajectories with colour coded particle energy for $K_{\rm res} = 100$ (Resistive mode). Grey lines show the initial magnetic field.

Simulations

Statistics

- Two simulations performed:
  - with 10^5 TP but less detailed integration – statistics
  - 10^4 TP with detailed integration – trajectories of individual particles studied
- Results for $K_{\rm res} = 10$.
  - Electron acceleration efficiency: $N_{E>10^{3.5}\text{ eV}}/N$ = 1.27%
- Results for $K_{\rm res} = 100$.
  - Electron acceleration efficiency: $N_{E>10^{3.5}\text{ eV}}/N$ = 2.18%

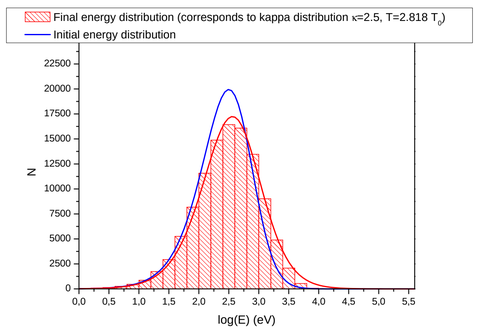

Figure 5: Final electron energy distribution (for $K_{\rm res} = 10$).

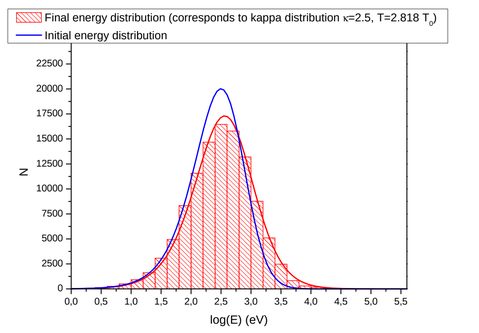

Figure 8: Final electron energy distribution (for $K_{\rm res} = 100$).

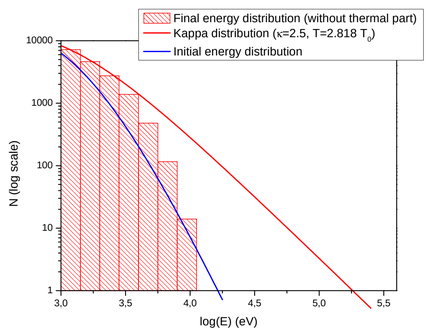

Figure 6: Final electron energy distribution (for $E > 1$ keV and $K_{\rm res} = 10$).

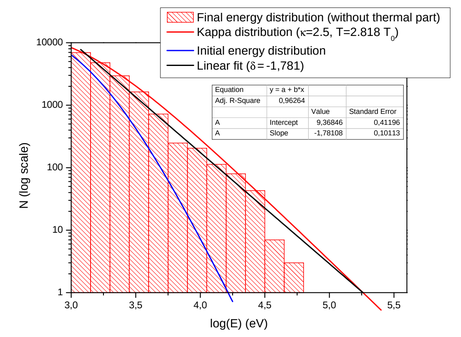

Figure 9: Final electron energy distribution (for $E > 1$ keV and $K_{\rm res} = 100$).

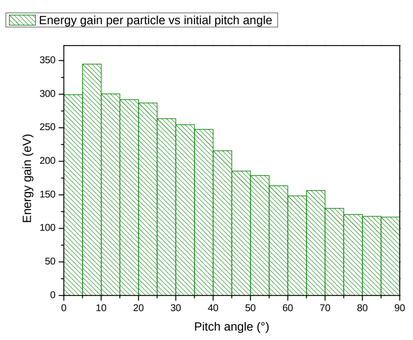

Figure 7: Distribution of energy gain per electron vs initial pitch angles (for $K_{\rm res} = 10$).

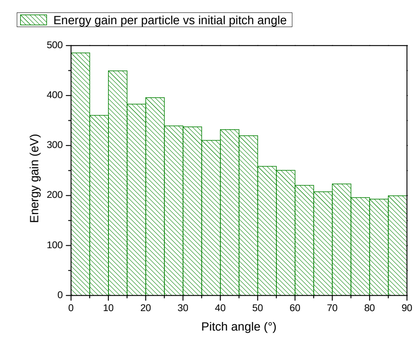

Figure 10: Distribution of energy gain per electron vs initial pitch angles (for $K_{\rm res} = 100$).

Electron trajectories

- In Figure 11 typical trajectories for $K_{\rm res} = 10$ are shown. Acceleration in turbulent magnetic field dominates here.
- In Figure 12 typical trajectories for $K_{\rm res} = 100$ are shown. Acceleration in resistive DC field dominates here.
- In Figure 13 trajectories of selected few particles accelerated above 5 keV (for $K_{\rm res} = 100$) are shown. Both types of acceleration are relevant.

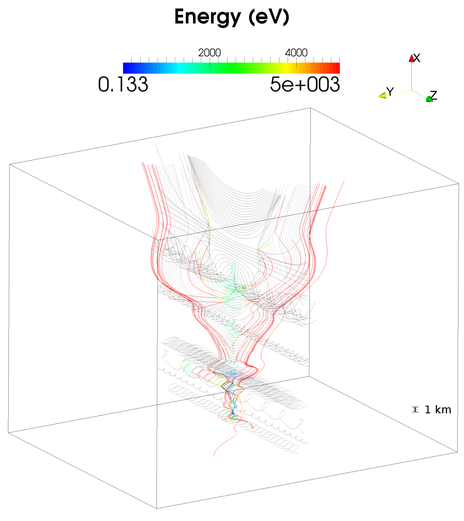

Figure 13: Acceleration of individual electrons within the current sheet for $K_{\rm res} = 100$. Changing colours of electron trajectories code their instant kinetic energy. Grey lines show the initial magnetic field.

Summary of results

- We identified two accelerating mechanisms. Electron acceleration caused by DC resistive electric field and stochastic acceleration due to the 'turbulent' nature of magnetic field within the current sheet.
- The turbulent magnetic field (even with $K_{\rm res} = 0$) accelerates electrons to low energies $E < 5$ keV.
- The magnitude of the DC resistive field is influenced by the choice of the factor $K_{\rm res} \in (10, 10^3)$. The resistive DC fields are responsible for acceleration of particles to higher energies $E > 5$ keV. $K_{\rm res}$ thus influences the energy distribution of non-thermal electrons.

Conclusions

- Our preliminary results show, that there are two basic mechanisms of acceleration - acceleration caused by DC resistive field and acceleration caused by 'turbulent' nature of magnetic field within the cascading current sheet.
- $\mathbf{E}_{\rm res}$ is responsible for acceleration of electrons to higher energies ($E > 5$ keV), whereas turbulent magnetic field accelerates electrons mainly to lower energies ($E < 5$ keV).
- In the future, we plan to investigate the role of individual regions and processes responsible for electron acceleration in a detail. We also plan to extend our simulations by including larger spatial scales.

References

Bárta, M. et al., 2011a, ApJ, 730, 47

Bárta, M. et al., 2011b, ApJ, 737, 24

Büchner, J. et al., 2006, Physics of Plasmas, 13, 082304

Gordovskyy, M. et al., 2010, ApJ, 720, 1603

Hyman, A.-T., 1997, Am. J. Phys., 65, 3

Northrop, T.-G., 1963, The Adiabatic Motion of Charged Particles

Vay, J.-L., 2008, Physics of Plasmas, 15, 056701